

Polarized basolateral cell motility underlies invagination and convergent extension of the ascidian notochord

Edwin M. Munro^{1,2} and Garrett M. Odell¹

¹Department of Zoology, University of Washington, Seattle, WA 98195, USA

²Friday Harbor Labs, Friday Harbor, WA, 98250, USA

*Author for correspondence (e-mail: munroem@u.washington.edu)

Accepted 5 October 2001

SUMMARY

We use 3D time-lapse analysis of living embryos and laser scanning confocal reconstructions of fixed, staged, whole-mounted embryos to describe three-dimensional patterns of cell motility, cell shape change, cell rearrangement and tissue deformation that accompany formation of the ascidian notochord. We show that notochord formation involves two simultaneous processes occurring within an initially monolayer epithelial plate: The first is invagination of the notochord plate about the axial midline to form a solid cylindrical rod. The second is mediolaterally directed intercalation of cells within the plane of the epithelial plate, and then later about the circumference of the cylindrical rod, that accompanies its extension along the anterior/posterior (AP) axis. We provide evidence that these shape changes and rearrangements are driven by active extension of interior basolateral notochord cell edges

directly across the faces of their adjacent notochord neighbors in a manner analogous to leading edge extension of lamellapodia by motile cells in culture. We show further that local edge extension is polarized with respect to both the AP axis of the embryo and the apicobasal axis of the notochord plate. Our observations suggest a novel view of how active basolateral motility could drive both invagination and convergent extension of a monolayer epithelium. They further reveal deep similarities between modes of notochord morphogenesis exhibited by ascidians and other chordate embryos, suggesting that cellular mechanisms of ascidian notochord formation may operate across the chordate phylum.

Key words: Notochord, Cell motility, Morphogenesis, Ascidian

INTRODUCTION

The active rearrangement of cells along one or more axes within a tissue to cause its extension along another, orthogonal axis is one of the fundamental morphogenetic engines of metazoan development. Examples of this convergence and extension engine appear throughout metazoan phylogeny in both mesenchymal and epithelial tissues including, primordial insect limbs (Fristom and Fristom, 1976), axial mesoderm and neural tissues in chordates (Keller et al., 1989; Keller et al., 1992; Keller et al., 1985; Miyamoto and Crowther, 1985; Schoenwolf and Alvarez, 1989; Thorogood and Wood, 1987; Trinkaus et al., 1992; Warga and Kimmel, 1990) and the sea urchin archenteron (Ettensohn, 1985; Hardin, 1989).

In the above examples, direct observations have established convergent extension as an autonomous process in which the tissue itself produces locally the forces responsible for deforming it. Observations of cell motility during rearrangements *in situ* reveal many similarities to how isolated cells move *in vitro* (Cooper and Kimmel, 1998; Elul et al., 1997; Hardin, 1989; Miyamoto and Crowther, 1985; Shih and Keller, 1992a; Trinkaus et al., 1992). These observations, and the phylogenetic conservation of core molecular machinery responsible for cell motility and adhesion, suggest that

universal cellular mechanisms may underlie convergent extension in divergent embryonic contexts.

However, convergent extension movements within embryos are necessarily collaborative efforts in which every cell simultaneously senses, exerts forces upon, and experiences forces from, all neighboring cells. To understand these collaborative rearrangements, we must understand how cell-cell interactions and tissue geometry constrain and organize the forces generated by individual cells to produce specific global patterns of cell rearrangement and tissue deformation. A fundamental step towards achieving this goal is to characterize, in specific case studies, the morphogenetic properties of cells in relation to the embryonic context in which they operate, and the global patterns of morphogenetic movement they collectively produce. Unfortunately, the size, cell number or opacity of many embryos makes doing so impossible.

Here, we exploit unique features of ascidian embryos to describe the three-dimensional patterns of cell motility, shape change and rearrangement that accompany notochord formation in the ascidians *Boltenia villosa* and *Corella inflata*. The ascidian notochord consists of exactly forty cells that transform in only 6 hours without cell divisions from a monolayer epithelial sheet into a rod of cells stacked end to end to form the structural core of the larval tadpole tail (Cloney,

1964; Conklin, 1905; Miyamoto and Crowther, 1985; Nishida, 1987; Satoh, 1993). This transformation involves convergent extension movements, but they occur in an embryo of less than a thousand cells against a background of invariant cell lineages and highly stereotyped development. The diminutive size of the ascidian embryo makes it possible to view the entire process with high numerical aperture lenses, and the optical clarity of *Corella inflata* makes it possible to do so in living embryos.

Early studies of living embryos were restricted to single focal planes, and limited by the inability of DIC optics to resolve local motile processes within close-packed tissues (Cloney, 1964; Miyamoto and Crowther, 1985). To overcome these limitations, we devised methods to record and then later retrieve and analyze time-lapse information at multiple focal heights within the same embryo, and thereby to reconstruct the complete sequence of cell shape changes and rearrangements in three dimensions within whole notochords in intact embryos. We also developed methods to preserve and visualize the actin cytoskeleton using confocal microscopy within whole-mounted embryos, and to fracture embryos and view the apical, basal, and basolateral surfaces of notochord cells directly with SEM. Together, these methods reveal both cellular architecture of the embryo as a whole and motile processes within individual cells allowing us to corroborate and extend our live time-lapse data and to correlate expression of local motile behavior with local organization of the actin cytoskeleton and local cell shape changes within the notochord.

MATERIALS AND METHODS

Animal collection and embryo culture

We collected *Boltenia villosa* and *Corella inflata* adults from Puget Sound. We isolated *Boltenia* gametes according to the method of Coombs et al. (Coombs et al., 1992). We removed chorions from mature eggs enzymatically by brief incubation in 1% sodium thioglycolate and 0.1% protease at pH 10, followed by 3 rinses in filtered sea water (FSW). We then fertilized the eggs in FSW at pH 10 by adding 0.5-1 ml concentrated sperm. We maintained developing embryos in FSW at 9-13°C in Petri dishes coated with Sylgard or a thin layer of 1% agarose.

To isolate *Corella inflata* gametes, we extruded sperm from the spermiduct and obtained primary oocytes by gentle maceration of the gonads. We allowed primary oocytes to mature for 1-2 hours at 10°C, removed chorions by brief incubation in 1% protease, then fertilized and cultured them as above.

3D time-lapse microscopy

We observed living embryos using a modified Kiehart chamber (Kiehart, 1982). All glass surfaces were coated with a thin layer of agarized sylgard or 0.1% gelatin/0.1% formaldehyde (Sardet et al., 1989) to prevent embryos from sticking. A standard temperature control circuit (Horowitz and Hill, 1989) supplied current to a peltier cooling chip (Melcor Thermoelectrics, Trenton NJ) mounted on the chamber so as to maintain a fixed temperature at a thermocouple lead placed next to the embryo.

To collect 3D time-lapse data, we used a computer controlled image acquisition system designed and built around a Zeiss WL Standard upright microscope in our laboratory by Garrett Odell and Victoria Foe. We imaged embryos with standard Nomarski optics using 40× (NA=0.9), or 63× (NA=1.2) plan neofluor multi-immersion lenses

adjusted for water immersion. We collected images using a Hamamatsu C2400 CCD camera and recorded frames processed through a digital frame grabber board (MaxVision, Datacube Inc, Peabody Ma) directly onto Hi8 video tape at 30 frames/second using a Sony EVO-9650 animation recorder. An IBM PC computer controlled both the frame grabber board and a digital stepper motor affixed to the fine focus knob of the microscope. Custom-written software synchronously controlled the stepper motor and the frame grabber board so as: (i) To produce a fixed user-specified increment in focus (approx. 0.3 μm) per video frame, phased to occur between frames. (ii) To pass each digitized frame through an internal buffer to be stamped with a binary grayscale pattern, written in the overscan region of the image, encoding the focal height, sweep number, and absolute time associated with that frame.

This system allows us to complete an entire focus sweep in approx. 3-10 seconds, collecting 30 optical sections each second. The specific time depended on the incremental step size and the depth of the focus sweep. We then wrote software controlling the animation recorder from a NeXT computer through an RS232 interface to address, retrieve, and digitize frames from any desired series of focal heights/sweep numbers/times, and to either re-record them on Hi8 tape as time-lapse movies, or to save them as a digital image stack that could be imported to other programs for further analysis. Fig. 6 shows typical optical sections.

Reconstructions of cell trajectories and fates

To compile cell trajectories at different focal heights (Fig. 7), we imported DIC focus sweeps into NIH Image, and deduced approximate cell outlines near dorsal and ventral surfaces by 'focussing' up and down through those surfaces. We then used time-lapse sequences at each focal height to establish a correspondence between identified cells at successive time points.

To extract morphometric parameters from DIC focus sweeps we used NIH Image to trace a polygonal outline for cellular cross sections at dorsal, middle and ventral levels. From this polygonal data, we used built-in NIH functions to obtain: an area, a length and width (the major and minor axes, respectively, of a best-fit ellipse), and a 'center of mass'.

Histochemistry and confocal microscopy

We fixed embryos for 20-30 minutes at room temperature in 4% EM grade formaldehyde (Electron Microscopy Sciences, Ft. Washington, PA) in a buffer containing 50 mM EGTA, 100 mM Pipes, and 400 mM sucrose, adjusted to pH 6.9. We then rinsed embryos 3 times with phosphate-buffered saline (PBS) and incubated them in Bodipy-phalloidin (1 unit/200 μl; Molecular Probes, Eugene OR) in PBS + 0.2% Triton X-100 (PBST) either overnight at 4°C or at room temperature for 1-2 hours. We then rinsed embryos 3× in PBS, attached them to poly-L-lysine coated coverslips, inverted them over tape spacers onto 3×5 inch glass microslides, dehydrated them through an isopropanol series, and cleared them using Murray clear.

Image collection

We collected laser scanning confocal microscope (LSCM) images on a Biorad model 600 LSCM attached to an upright Nikon microscope using a Nikon 60× Plan Achromat oil immersion lens (NA 1.4). In general, we used a Kalman average of 6-10 3/4-second scans. Additional collection parameters appear in figure legends. We used Adobe Photoshop to colorize the images shown in Fig. 2, Fig. 3, Fig. 4.

To visualize F-actin rich protrusions, we collected LSCM z-series at 0.2 μm or 0.3 μm intervals (section thickness 0.3-0.4 μm), with gain and offset adjusted so the dimmest pixels were at approximately 10% of maximum intensity and the brightest pixels were just under saturation. Fig. 9 shows sample optical sections. We then imported the resulting stacks into NIH Image for further analysis (counting) of protrusions and to produce the stereo pairs shown in Fig. 10.

Scanning electron microscopy

We fixed embryos for SEM in 2% gluteraldehyde in FSW for 2-4 hours at room temperature, rinsed them several times in FSW, and then post-fixed them in 1% osmium tetroxide (Electron Microscopy Sciences, Ft. Washington, PA) in FSW for 1-2 hours at room temperature. We then rinsed them briefly in distilled water, dehydrated them in ethanol, and critical point dried them at room temperature in hexamethyl disilizane (Sigma), mounted them onto SEM stubs coated with a single layer of double stick tape, and fractured them using a small piece of razor blade affixed to a wooden applicator. In some cases, we fractured embryos following the primary fixation step and then processed them as described above. We imaged specimens on a JEOL JSM-35 SEM microscope and captured selected images on Polaroid 55 film. To prepare final figures, we scanned either the positives or the negatives on a scanner (AGFA, Ridgefield Park, NJ) and then adjusted image intensity histograms to maximize contrast using Adobe Photoshop.

RESULTS

Confocal analysis of fixed and staged *Boltenia villosa* embryos

Fig. 1 summarizes the developmental period and the schedule of developmental events considered here, as they occur in *Boltenia* embryos at 10°C. For descriptive clarity, we group these events into three stages.

Stage I (early neurulation: 15-16 hours): oriented cell divisions and contraction of the posterior notochord boundary establish the initial shape of the notochord plate

The final round of notochord cell divisions begins about 30

minutes after neurulation starts (15 hours after fertilization; AF). At this time, the presumptive notochord comprises an epithelial sheet of exactly 20 cells arranged as two semi-circular arcs around the anterior lip of the blastopore (Fig. 2). The middle eight cells in each arc [the primary lineage: descendants of the A4.1 blastomeres (Conklin, 1905; Nishida, 1987)] divide first, then the lateralmost cells [the secondary lineage: descendants of the B4.1 blastomeres (Conklin, 1905; Nishida, 1987)] divide approximately 30 minutes later. All cells divide perpendicular to the original arcs, transforming 2 rows into 4 (Fig. 3, left column). During this same time, the apices of primary notochord cells at the blastopore lip gradually constrict and disappear, and the lateral ends of anterior notochord arcs bend posteriorly and towards the midline to enclose these cells within the plate's interior, joining the strands of secondary cells at the posterior midline (Fig. 3A). Also during the final division, the lateral edges of the notochord plate fold ventrally to lie beneath the main plate, possibly driven by the lateral spreading of notochord cell arcs as they divide (Fig. 3J). Often cells lying at or near the lateral fold position withdraw their apices into the notochord interior but retain contact with the basal notochord surface; otherwise all notochord cells remain within a contiguous monolayer.

Stage II (middle-late neurula: 16-18.75 hours). The notochord invaginates to form a cylindrical rod while individual cells elongate and intercalate within the monolayer and perpendicular to the AP axis

During stage II, the notochord begins to extend along the AP axis (Fig. 3, top 3 rows). Below the apical surface, cells elongate perpendicular to the AP axis, shorten along it, and repace in a convergent extension fashion (Fig. 3A-C). Similar

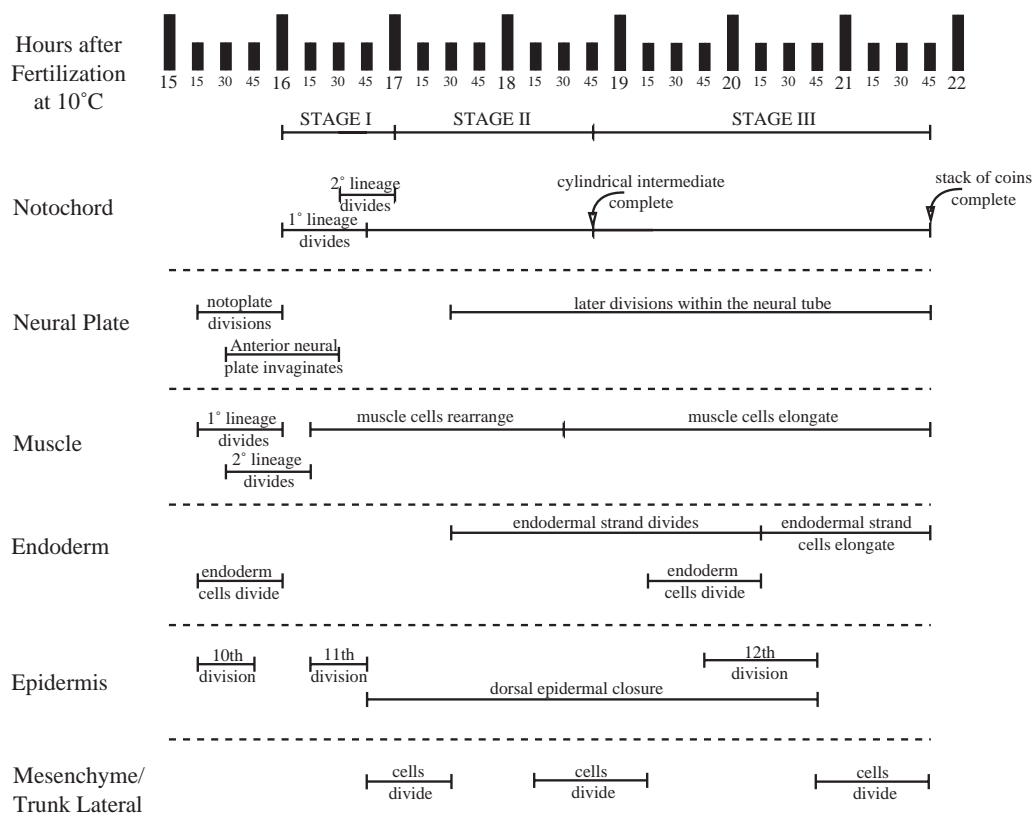
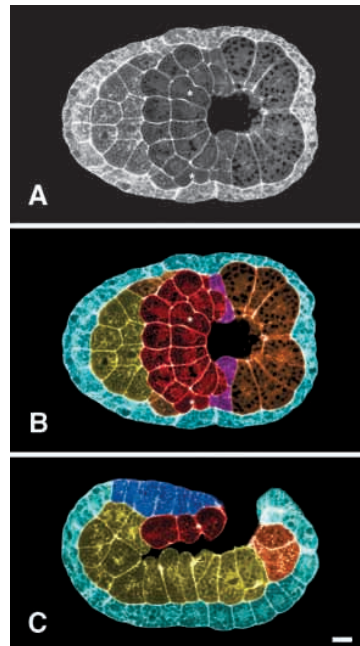


Fig. 1. Timeline showing major morphogenetic events at 10°C in *Boltenia villosa* between late gastrulation, approx. 14 hours after fertilization (AF), when notochord cells begin to divide for the final time, and tailbud stage when notochord cells have completed their rearrangements to form a stack of coins. We analyzed at least 6 and typically more than 10 embryos at each time point. Labeled segments associated with a given event span the period in which we observed that event in one or more embryos. The actual intervals in which that event occurs may be shorter.

Fig. 2. Colorized confocal sections taken from whole-mounted phalloidin-stained *Boltenia villosa* embryos at selected stages. Dorsal is always up. In top and side views, anterior is to the left and posterior to the right. Red=primary notochord lineage; violet=secondary notochord lineage; dark blue=neural plate; orange=posterior muscle; light brown=mesenchyme/trunk lateral cells; yellow=endoderm/endodermal strand; light blue=epidermis. Scale bar, 10 μ m in all panels. The above also refers to Fig. 3 and Fig. 5. A late gastrula stage embryo (approx. 15 hours AF). (A) Raw confocal data before false coloring to produced B; (B) Top view; (C) Lateral view. Several cells within the primary notochord lineage have just begun to cleave (asterisks). Secondary notochord lineage cells (violet) lie at the ends of the notochord plate just anterior to the posterior muscle. Note that apices of individual cells forming the anterior portion of the blastopore lip have not yet begun to constrict.

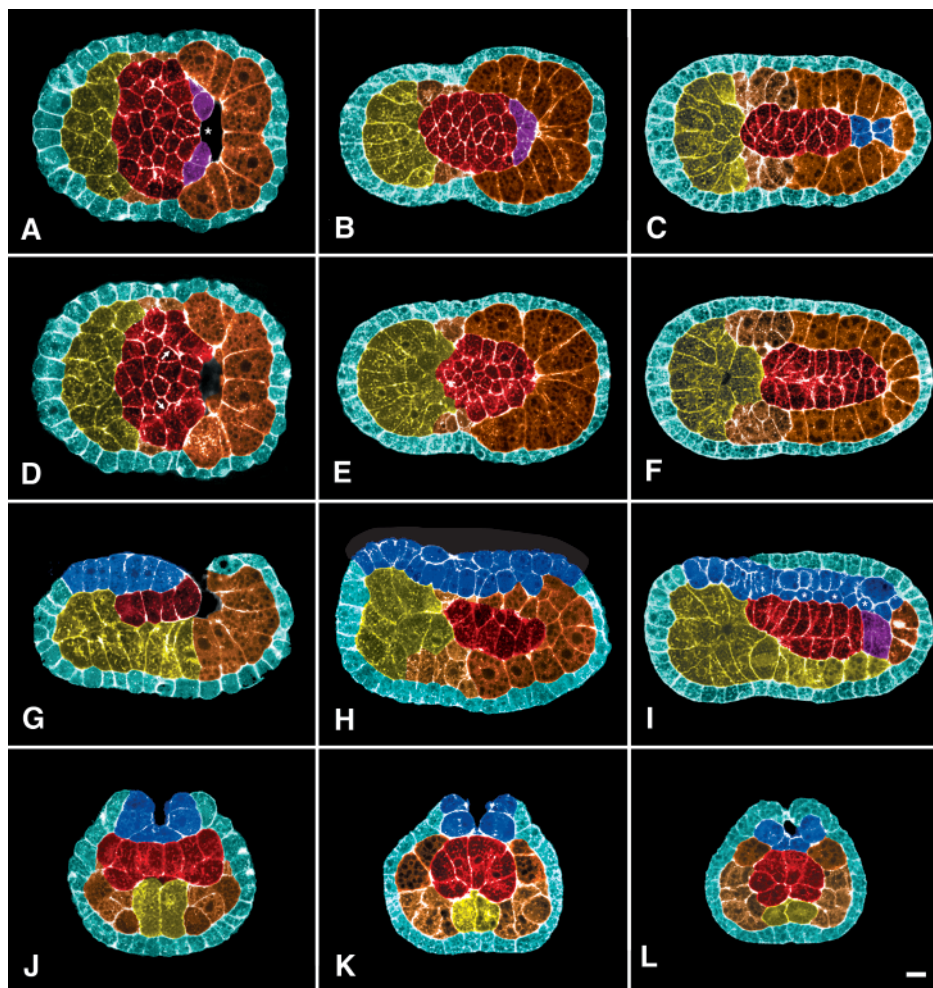


shape changes occur across the entire width of the notochord plate and around the lateral folds (compare Fig. 3B and 3H). Cell apices also repack, but they remain roughly isodiametric and their areas decrease as the notochord plate invaginates (Fig. 3D,E).

At the same time, the notochord invaginates about the axial midline to make a cylindrical rod (Fig. 3J-L). At the anterior, where neural folds are less pronounced, curvature increases steadily and uniformly across the width of the notochord plate and individual cells within the plate become increasingly wedge shaped in cross-sectional profile (Fig. 3J-L). At the posterior, the outer (basal) boundary of the notochord plate, initially sharply folded at its lateral edges, adopts a progressively

more uniform curvature (not shown). Also the lateral folds move towards and fuse at the ventral midline, first at the posterior and then at progressively more anterior positions (Fig. 4).

Fig. 3. Confocal sections from embryos at late stage I (left column; approx. 16 hours AF), mid-stage II (middle column; approx. 17 hours AF) and early stage III (right column; approx. 18 hours AF). (A-C) Dorsal notochord plate. (D-F) Ventral notochord plate. Arrows indicate the lateral folds in D. In A, the secondary notochord cells (violet) are just rounding up to divide. Many primary cells have lost contact with the blastopore lip and joined the interior of the notochord plate, while others have greatly constricted apices (asterisks). (G-I) Lateral sections through the notochord plate. G and I show midline views. H shows a more lateral view to illustrate how cells at the lateral invaginating edges of the notochord plate are also elongated perpendicular to the AP axis. Note how the dorsal (basal) ends of many individual cells in I tend to extend posterior relative to the ventral (apical) ends of the same cells. The same phenomenon is apparent in F. The apices of these cells tend to become stretched along the AP axis by early stage III (not shown). Asterisks in I mark dividing cells within the neural tube. (J-L) Cross sections through the notochord plate taken near its anterior end where the lateral folds are least pronounced and the invagination progresses simultaneously across the width of the plate.



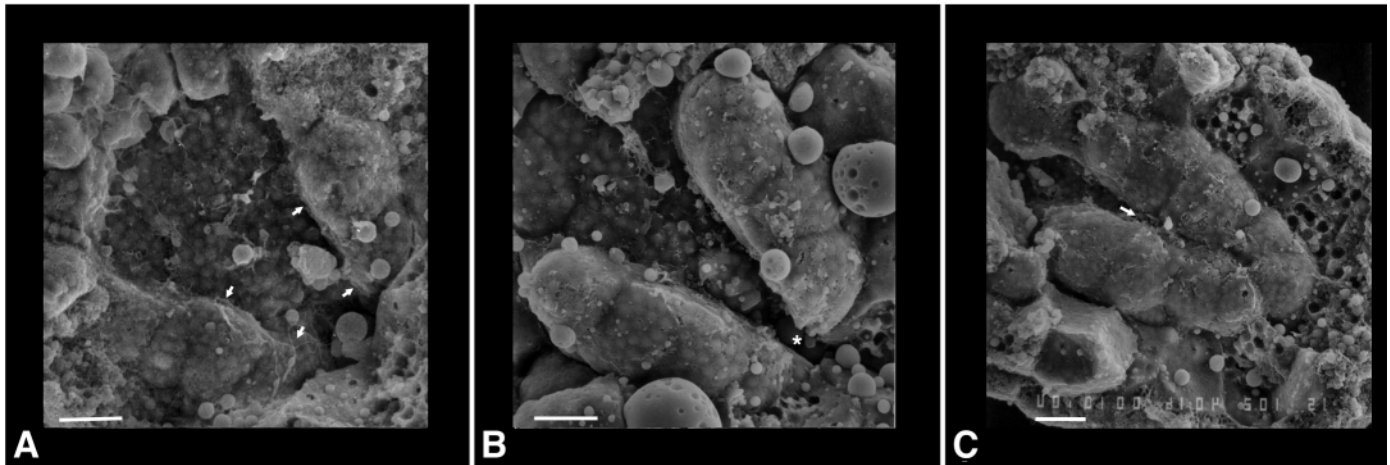


Fig. 4. SEM views of *Boltenia villosa* embryos fractured to reveal the apical (ventral) surface of the notochord plate and the ventral folds at: (A) approx. 16 hours AF; (B) approx. 17 hours AF and (C) approx. 18 hours AF. Folds are present before cell rearrangement and notochord extension occurs (arrows in A), and then move towards the midline, meeting first at the posterior (asterisk in B) where they begin to fuse. Fusion then progresses posterior to anterior (fusion ‘front’ indicated by arrow in C). Posterior is top and left in all panels. Scale bar, 10 μm .

Stage III (early tailbud, 18.75 – 21 hours). All cells intercalate about the circumference of the notochord cylinder as it elongates

When stage III starts, the notochord is a cylindrical rod except its most anterior end which remains flattened (Fig. 3, right column). Individual notochord cells have adopted ‘pizza slice’ shapes with their original basal ends forming the outer notochord boundary and their original apices lying near the notochord center along the original apical notochord surface, which persists well into stage III as a single densely phalloidin-stained line along the center of the notochord axis (not shown). Over the next 3 hours, the number of cells seen in cross section at a given axial position decreases steadily as each cell’s basal end extends around the cross-sectional circumference of the notochord until each cell is coin-shaped and all cells stack single file along the rod (Fig. 5). Subsequently individual cells vacuolate and swell, driving further extension of the notochord and tail (Cloney, 1964; Miyamoto and Crowther, 1985).

Mediolateral cell intercalation within a monolayer epithelium drives notochord extension

To analyze cell intercalations during notochord formation, we used 3D time-lapse microscopy (see Materials and Methods) to identify and follow every notochord cell within a single *Corella* embryo from early stage I to just before the end of stage III (Fig. 6). Fig. 7 shows outlines of identified cells near the dorsal and ventral surfaces at early stage I, late stage II, and late stage III. Cells intercalated perpendicular to the AP axis within the dorsal plate, between dorsal plate and lateral folds and, when lateral folds fused at the ventral midline, across that midline. In all cases, intercalations

occurred between immediately adjacent neighbors within the plane of the original notochord monolayer. Even at later stages, when the apical surface has been internalized, notochord cells rarely if ever extended across this apical centerline until they come to occupy a full half of the notochord circumference, at which point they extended rapidly across the rest.

Existing models for cell rearrangement within epithelia make different predictions about where the first contact between intercalating cells should be established (Fristrom, 1982; Jacobson et al., 1986). Fristrom’s biased apical contraction model (Fristrom, 1988; Fristrom, 1982) implies that contacts should be established first at the apical surface, while Jacobson et al.’s Cortical Tractor Hypothesis (Jacobson et al., 1986) implies that contacts should initiate near the basal surface and then propagate apically. We therefore examined where contact is first established between intercalating cells in the notochord plate. In all intercalation events we examined ($n=19$), the first contact between intercalating cells occurred well within the interior of the notochord plate, and then propagated towards the basal and apical surfaces.

Notochord cell extension and intercalation is polarized relative to both the AP and apicobasal axes of the notochord plate

To further characterize mediolateral intercalation, we measured changes in cross-sectional cell shape and position at three heights along the apical-basal axis: just below the apical surface (apical); just above the basal surface (basal); and

Fig. 5. Progressive intercalation of cells within the cylinder during mid-late stage III (approx. 18–21 hours AF). Cross sections A–D are taken from different embryos at progressive stages to illustrate the expansion of wedge-shaped cells about the circumference of the notochord rod.

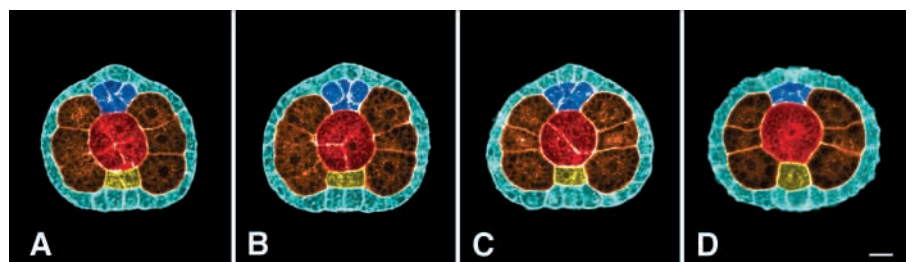
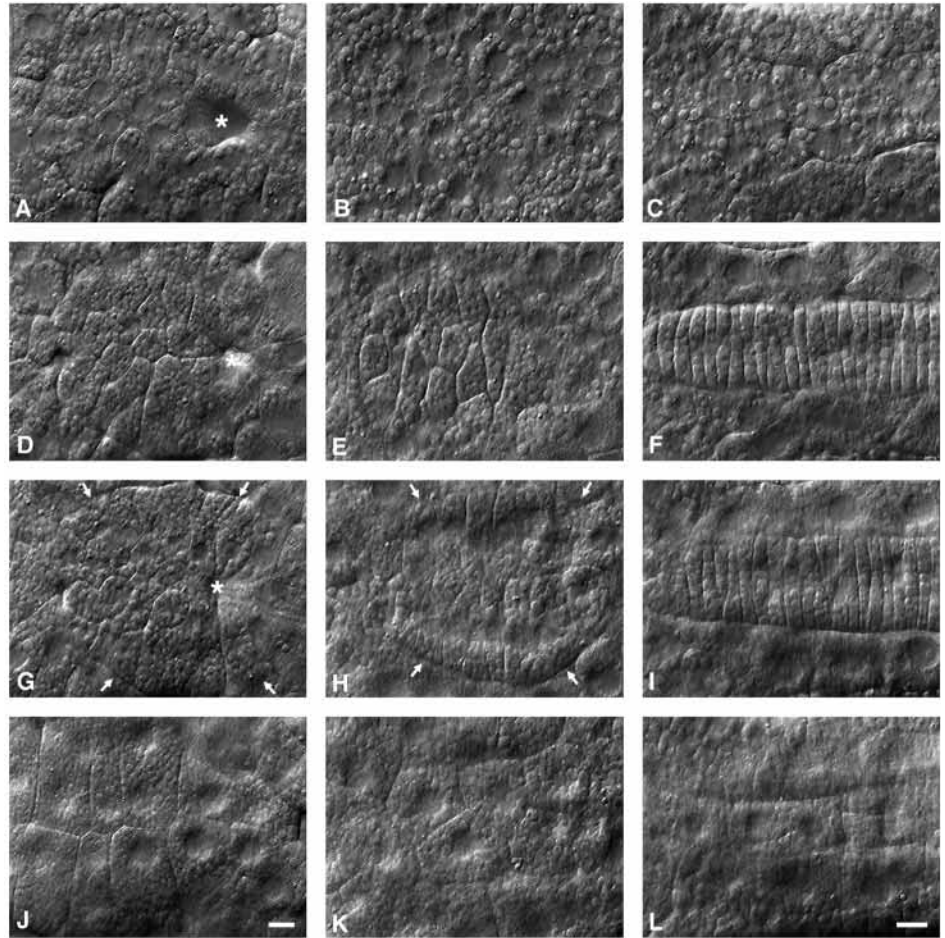


Fig. 6. DIC sections taken from focus sweeps through a living *Corella inflata* embryo at three successive stages. (A-C) Sections through the neural plate/tube. (D-F) Sections through the dorsal notochord plate/cylinder/rod. (G-I) Sections through the dorsal notochord plate/cylinder/rod. (J-L) Sections through the endodermal strand. First column (A,D,G,J) just after completion of the final notochord cell division. Second column (B,E,H,K) mid-neurula stage, approximately 2 hours after the completion of the final division. Third column (C,F,I,L) stack of coins stage, approximately 6 hours after completion of the final division. By this stage, approximately half of the notochord has extended posterior beyond the field of view. Anterior is to the left in all panels. Asterisks in A,D,G mark the blastopore. Arrows in G and H indicate the boundaries of the notochord. Scale bar, 10 μ m.



equidistant between the apical and basal surface (middle) (Fig. 8; see Materials and Methods). Cross-sectional length/width ratios increased steadily within basal (and middle) cross sections from 1.43 (and 1.36) near the end of stage I to 2.3 (and 2.09) near the end of stage II. Cell lengths increased and cell widths decreased, while cross-sectional areas decreased slightly. In contrast, apical cross-sectional length/width ratios

remained roughly constant while cross-sectional lengths, widths and areas decreased steadily (Fig. 8).

To quantify relative movements of cells during intercalation, we computed the average distance between centers of mass of neighboring cells during late stage I and early stage II ($n=15$ cell pairs), dividing by cell lengths to normalize for changes in center distance produced by coordinate shape change rather than relative cell movement (e.g. convergence of apical cell centers produced by uniform shrinkage of all cell apices; see Materials and Methods for details). The resulting normalized center distance decreased steadily throughout late stage I and II (Fig. 8), showing that the emergence of polarized cell shape changes are accompanied from the outset by relative movements of cells across one another's surfaces. Normalized

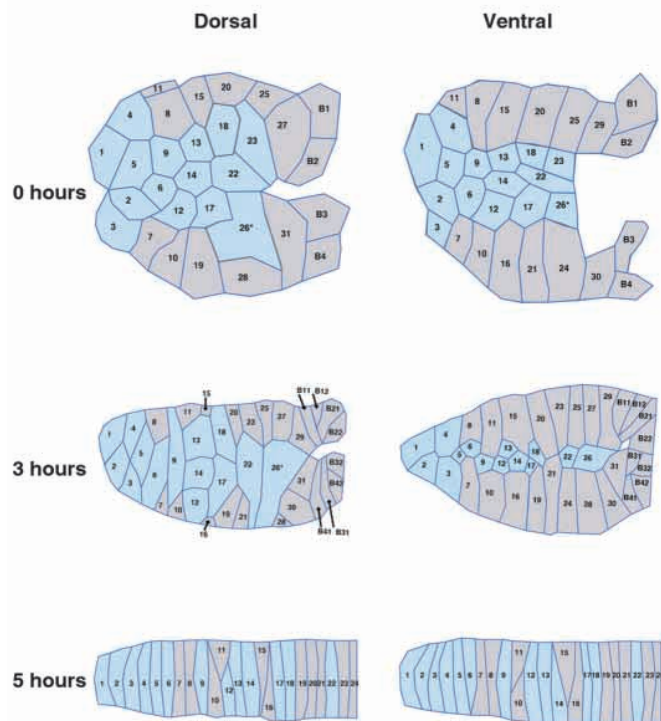


Fig. 7. Reconstruction of cell movement and shape change during notochord formation in a living *Corella inflata* embryo (the same shown in Fig. 6). Cell outlines represent approximate cell boundaries as seen in cross section near the dorsal surface (left column) or ventral surface (right column) of the notochord plate. Anterior is to the left in all panels. Times shown are from completion of the final primary division. Blue cells remained within the dorsal plate; Grey cells started within or intercalated into the ventral folds. Cells 1-31 derive from the primary lineage. Cells B1-B8 derive from the secondary lineage. Cell 26 failed to divide for the last time but nevertheless changed shape and intercalated as other cells do. In the lowermost panels, part of the notochord has extended rightward out of the video camera's field of view.

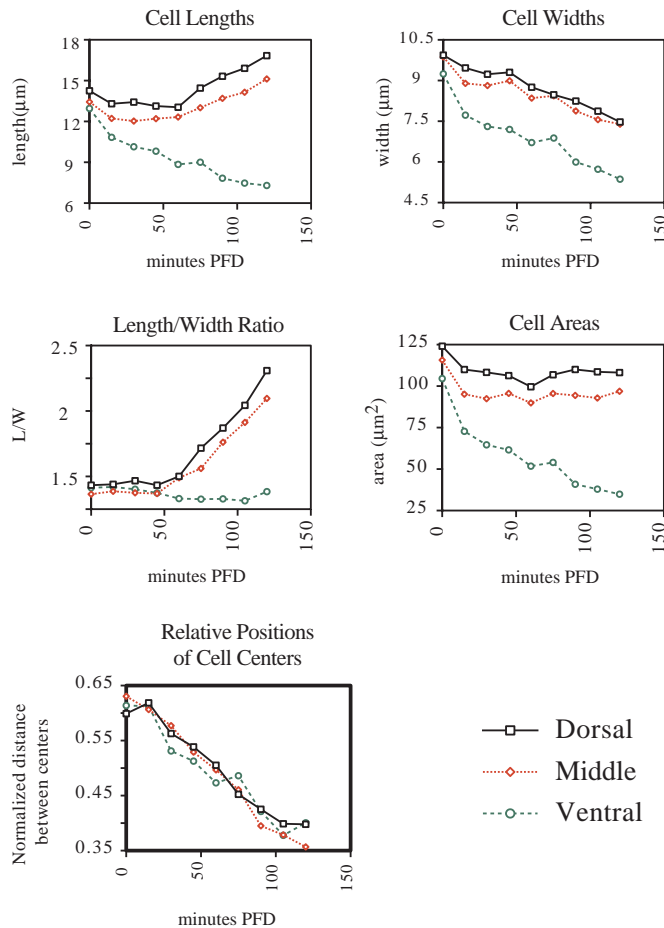


Fig. 8. Morphometric analysis of cross-sectional cell shape changes during notochord formation in a living *Corella inflata* embryo. In each graph, the time represents minutes elapsed since final cleavage in the primary lineage.

distance changes were very similar at apical, middle and basal levels, implying a greater absolute relative movement of cells at middle and basal levels.

The organization of F-actin in ascidian notochord cells reveals active basolateral crawling

Our DIC time-lapse movies revealed a general jostling of cells similar to that described by Myamoto and Crowther (Myamoto and Crowther, 1985). But we were unable to resolve localized motile behaviors that might account for the cell movements and shape changes we observed. Because filamentous actin (F-actin) has been implicated in the generation of motile force in nearly all cell types and is enriched in cellular structures associated with active protrusion and/or contraction, we decided to characterize its sub-cellular organization in ascidian notochord cells during active rearrangement.

Fig. 9A shows a medial LSCM section at early stage II when notochord cells are actively rearranging. At the basolateral cortex, F-actin appears as a patchy ring of intense stain, which grazing sections reveal to be a dense meshwork of interconnected fibres (Fig. 9C). 3D reconstructions of entire notochord plates reveal a similarly patchy cortical distribution across the entire basolateral surfaces of all notochord cells, but

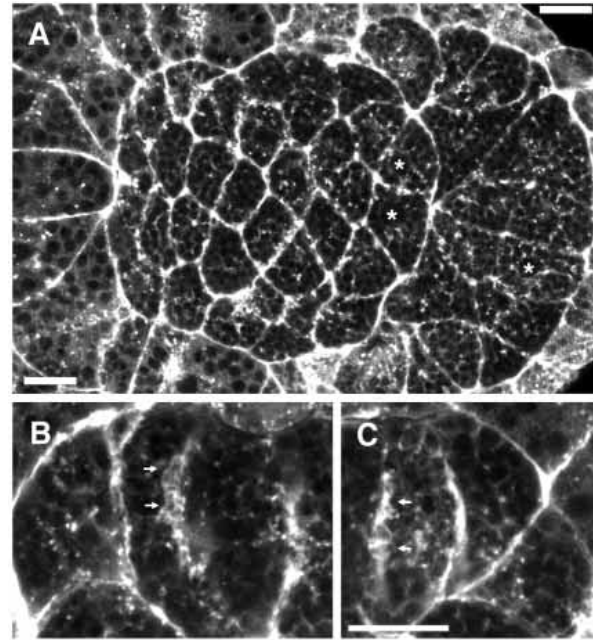


Fig. 9. F-actin organization within the notochord. Each image is a projection of 5 confocal sections taken at 0.2 μm intervals. (A) Top view section through a mid-stage II embryo (approx. 17 hours AF) illustrating general F-actin organization within the notochord plate and surrounding tissues. The interior cytoplasm of each notochord cell is filled with a dense meshwork of F-actin except where excluded by yolk granules (small dark holes) or nuclei (*). F-actin puncta similar to those described elsewhere (Foe et al., 2000; von Dassow and Schubiger, 1994) appear throughout the cytoplasm. Posterior is to the left. (B,C). Cross-sectional views of stage II embryos showing actin-rich protrusions (arrows) extending across the surfaces of adjacent neighbors. In C a protrusion lies just out of focus and to its right can be seen a dense meshwork of F-actin fibers in the cortex of the cell across which it is extending. Dorsal is up in B and C. Scale bar, 10 μm in all panels. B and C have same scale.

little or no difference in average density of F-actin along the apicobasal axis. Adjacent endoderm cells, which do not rearrange at these stages, exhibit a similar density and organization of internal actin, but the cortical actin is both more uniform and less dense, with an intensity of signal similar to that seen along the least dense sections of notochord cell cortices.

The brightest accumulations of F-actin within the notochord plate occur at interior junctions made by three or more notochord cells, where dense bands of F-actin run the apical-to-basal length of each notochord cell. Similar accumulations occur in the mid-gastrula stage notochord and in anterior endoderm cells but they are far brighter in notochord cells when they are rearranging. Transverse grazing sections which pass through three cell junctions (Fig. 9B,C), or 3D reconstructions of notochord plates (Fig. 10), show these accumulations lie within lamelliform extensions of individual interior notochord cell edges. These extensions become larger and more numerous as cells begin to converge and extend, and they also become more obviously biased to medial and lateral edges (compare Fig. 10A,B; Table 1). Between late stage I and mid stage II, the fraction of basolateral edges bearing detectable protrusions increased from 0.27 ± 0.04 ($n=5$)

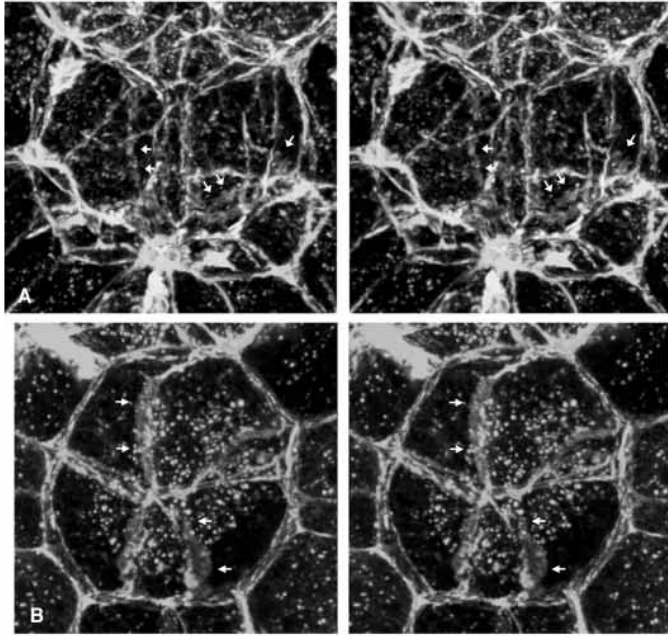


Fig. 10. Stereo views of F-actin-rich protrusions within the notochord rudiment. (A) Cross-sectional view through the notochord of a mid-late stage 2 embryo. (B) Cross section through an early-mid stage III embryo. Arrows in each panel indicate individual protrusions.

embryos) to 0.46 ± 0.11 ($n=5$ embryos). At stage I, there was a weak but non-significant ($P=0.08$, Student's *t*-test) bias towards protrusions being oriented mediolaterally. By early-mid stage II, however, a clear bias had emerged ($P<0.02$). By early stage III when cells have adopted their typical pizza slice morphology, nearly every medial or lateral edge bears a broad flattened lamellar protrusion (Fig. 10B).

SEM analysis of interior and surface protrusions

To corroborate our confocal observations, we viewed transverse fractures of fixed embryos using scanning electron microscopy (SEM) (Fig. 11A,B). In fractures that pass cleanly between neighboring cells, we could often see flat lamelliform protrusions extending across the faces of adjacent cells. These protrusions, devoid of yolk granules, have roughly the same dimensions as the F-actin-rich protrusions seen in confocal preparations.

At the apical surface, cells make very short protrusions across the surfaces of adjacent cells that tend to interlock with

Table 1. Distribution of interior protrusions within the notochord plate during early stages of notochord formation

	F_{total}	F_{perp}	F_{par}
Stage I	0.27 ± 0.04	0.32 ± 0.06	0.22 ± 0.09
Stage II	0.46 ± 0.11	0.59 ± 0.08	0.32 ± 0.15

Perpendicular edges are interior edges whose orientation lies within 45° of perpendicular to the AP axis. Parallel edges are interior edges that lie within 45° of parallel to the AP axis. F_{total} : fraction of total interior edges bearing F-actin-rich protrusions. F_{perp} : fraction of perpendicular edges bearing F-actin-rich protrusions. F_{par} : fraction of parallel edges bearing F-actin-rich protrusions. Data taken from 5 embryos at each stage.

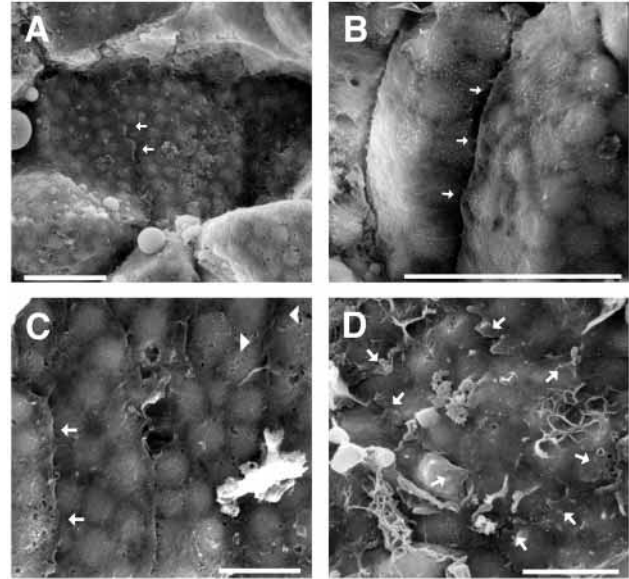


Fig. 11. SEM views of notochord cell protrusions. (A,B) Cross-sectional views of mid-stage II (A) and early stage III (B) embryos. Arrows indicate individual protrusions. Bright spots are yolk granules lying just under the membrane. (C) Outer (basal) surface of an early stage III embryo. In most (see arrows) but not all (arrowheads) cases, cells extend long continuous protrusions across the surfaces of adjacent neighbors. (D) Ventral surface of a late stage I embryo. Adjacent cells extend short interlocking protrusions across one another's surfaces. Arrowheads outline a single cell, indicating in each case the direction of the protrusion. Scale bars, 10 μm in A and B and 5 μm in C and D. Dorsal is up in A and B.

one another (Fig. 11D). Basally, (at least at early stage III when we were able to obtain clean fractures) protrusions extend more continuously along boundaries between adjacent cells so one cell tends to continuously overlap its neighbor (Fig. 11C). In a given embryo, most overlapping protrusions were oriented in the same direction along the AP axis giving the basal surface a shingled appearance. However, the direction of overlap differs from one embryo to the next.

DISCUSSION

Ascidian notochord forms by simultaneous invagination and convergent extension within a monolayer epithelium

Our results show that ascidian notochord formation involves two simultaneous processes within a monolayer epithelium (Fig. 12A): invagination of the notochord plate to form a solid cylindrical rod; and convergent extension driven by active mediolateral intercalation of cells, first within the notochord plate and then later about the circumference of the solid rod. The final result is a single file of cells stacked end-to-end along the AP axis.

This mode of notochord formation is strikingly similar to that seen in many other chordate embryos including amphioxus (Conklin, 1928), urodele amphibians (Brun and Garson, 1984; Lofberg, 1974), and mouse (Sulik et al., 1994). In all of these cases, the notochord forms by invagination of the superficial

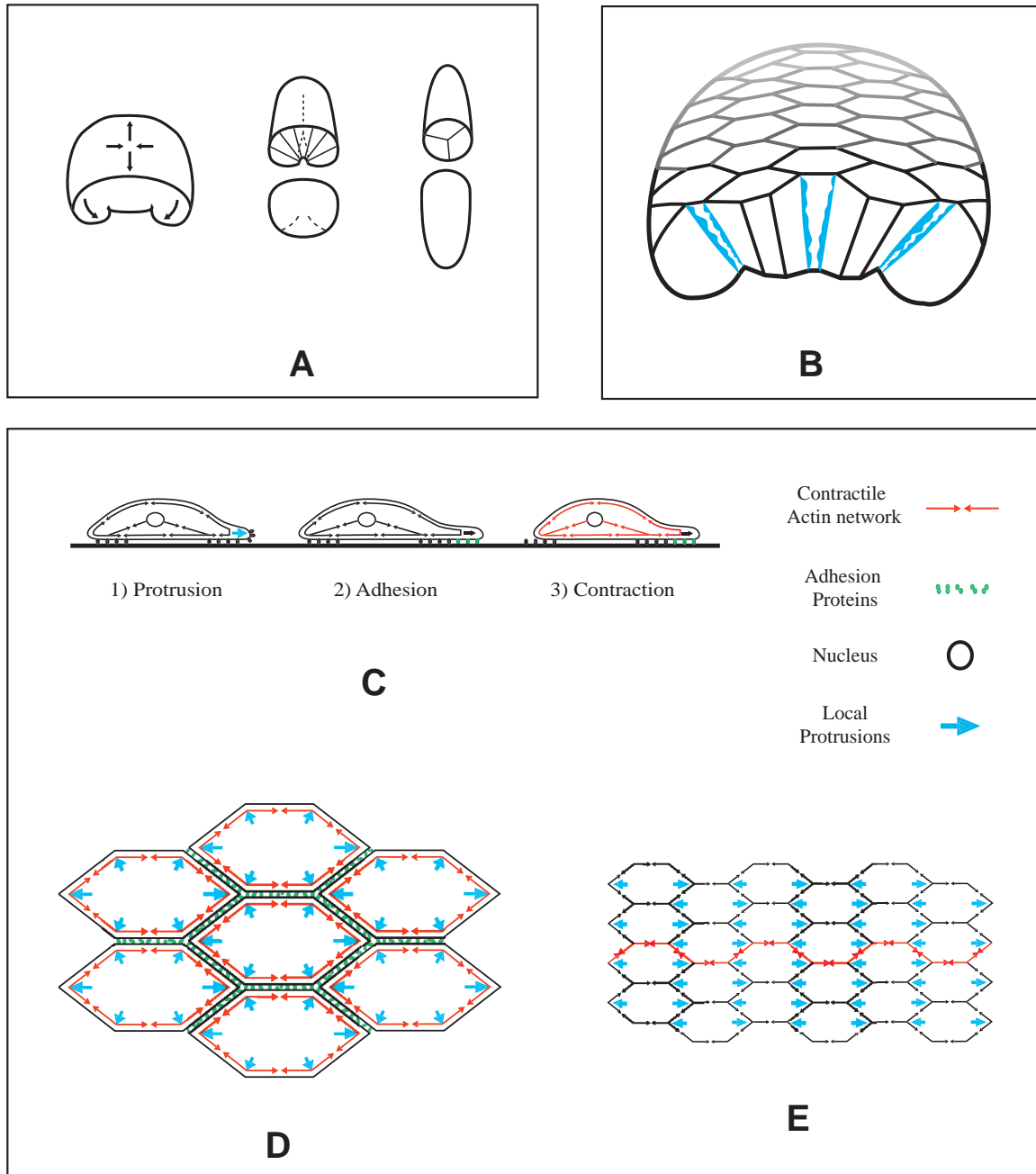


Fig. 12. (A) Invagination and convergent extension lead to formation of a cylindrical intermediate. Arrows at left indicate convergent extension movements of cells within the notochord plate and its invagination, which occur simultaneously during late stage I and stage II. Dorsal is down and ventral is up. (B). Schematic view of an early-mid stage II notochord plate showing how individual cells extend their interior edges across the faces of adjacent notochord cell neighbors. (C). Textbook view of how an isolated cell crawls on a flat external substratum. (1) Localized actin-dependent protrusive forces (blue arrows) cause the leading edge to extend relative to adhesive contacts with the underlying substratum; (2) New adhesive contacts (green ovals) form at the leading edge with the underlying substratum, and subsequently stabilize through various mechanisms, including lateral clustering of adhesion proteins, and association with the underlying cortical cytoskeleton; (3) actin/myosin-dependent contractile forces within the cortical or interior cytoplasm (red arrows) set up a tug of war between different sites of attachment to the substratum. Directional movement occurs when this tug of war is biased to favor consolidation of leading edge attachments and release of adhesions at the rear (Chen, 1981; Jay et al., 1995; Palecek et al., 1996). (D) How the same machinery might operate within a monolayer epithelium. Each polygonal cell represents a cross section through an epithelial cell somewhere below the apical surface, each vertex represents an interior (basolateral) edge, analogous to the leading edge in (C), which attempts to extend (blue arrows) between adjacent neighbors. Homophilic associations between cadherin proteins replace the integrin-based adhesion used by most mesenchymal cells, but the underlying mechanics are entirely analogous. For simplicity, we consider contractile forces only within the cortex. (E) Mediolaterally biased protrusion (blue arrows) drives cells away from their preferred circular cross-sectional shapes. The cortical contractile forces that act to restore these shapes within each cell (red arrows) are joined by adhesive contacts to make contractile chains that span the width of the notochord plate and cause it to become longer and narrower.

epithelium that forms the roof of the embryonic archenteron. This suggests that invagination coupled to convergent extension is an evolutionarily conserved mode of notochord morphogenesis and that insights we gain from studying notochord morphogenesis in the relatively simple context of the ascidian embryo may be applicable to other chordates.

Mechanisms of cell rearrangement within epithelia

Attempts to understand the mechanistic basis for active cell rearrangements within epithelia have focused on two basic questions (Fristrom, 1988; Gumbiner, 1996; Kolega, 1986; Speigel and Speigel, 1986): Where and how are the active forces responsible for cell movements and shape changes generated? And how do these forces bring together the boundaries of non-adjacent cells to cause the neighbor exchanges necessary for cell rearrangements while maintaining the close adhesive associations characteristic of epithelial sheets?

Direct observations of motile activity in epithelia have focussed on the exposed basal surfaces. These observations have revealed a range of local protrusive structures and behaviors, but it has been difficult to envision how they could produce observed patterns of cell shape change and rearrangement, leading some to suggest that the real action may occur elsewhere (Fristrom, 1988; Fristrom, 1982; Jacobson et al., 1986; Keller and Hardin, 1987). Jacobson and colleagues proposed a cortical tractor model in which a time-averaged cortical flow carries adhesive contacts from basal and basolateral regions towards the apical surface (Jacobson et al., 1986). They suggest cellular protrusions, which they and others have observed, extend across the basal or basolateral surfaces of the epithelium to establish novel contacts between non-adjacent cells which the cortical flow would then propagate to the apical surface. In this model, apical junctions turnover continuously and are replaced by junctional proteins that are inserted into basal and lateral membranes and carried apicalwards by the cortical flow, providing an elegant mechanism by which junctions between one pair of cells can replace those between another gradually and without loss of mechanical integrity or relative impermeability of the epithelium. This model is consistent with numerous observations of cortical flow in cultured cells (Bray and White, 1988) and polarized insertion/turnover of adhesion proteins and other cortical elements (Lawson and Maxfield, 1995; Palecek et al., 1996; Schmidt et al., 1995; Schmidt et al., 1993), but remains to be established for epithelial cells *in situ*.

An alternative hypothesis proposed by Fristrom (Fristrom, 1988; Fristrom, 1982) suggests that contractions of circumapical filament bundles, biased to specific apposing cell faces, could pull non-adjacent cell edges together to make novel contacts through special 4-cell junctional intermediates. In this view, cells rearrange without any shear between adjacent cell boundaries because they extend or shorten their common boundaries in a coordinated fashion. Fristrom's hypothesis is based on her own observations of cell rearrangements and junctional morphology underlying imaginal disc evagination in *Drosophila* (Fristrom, 1982), and is consistent with the demonstrated contractility of circumapical filament bundles (Owaribe et al., 1981).

Neither of these models is consistent with our observations. In the ascidian notochord, contacts between non-adjacent cells typically form interior to the notochord and then propagate

towards both the apical and basal poles, rather than flowing only basal-to-apical as the cortical tractor hypothesis asserts, or initiating apically as Fristrom's hypothesis implies. The short flattened basal protrusions that we observe at the basal surfaces of notochord cells do not extend far enough to establish novel contacts between non-adjacent cells as the cortical tractor hypothesis suggests. On the other hand, we find no evidence for an especially dense circumapical microfilament ring as others have described elsewhere, or for the biased accumulation of F-actin to particular interior cell faces.

A working hypothesis for active cell rearrangements within a monolayer epithelium

Our observations suggest an alternative hypothesis: that notochord cells move and change shape by crawling directly across the interior surfaces of their adjacent notochord neighbors using the same conserved cytoskeletal machinery, and the same basic mechanisms of motile force generation, that many other cells (e.g. fibroblasts and keratocytes) use to crawl across flat substrata *in vitro* (Fig. 12B-D).

Fig. 12C illustrates the current textbook view of how motile cells advance across an external planar substratum through a combination of, (1) actin-dependent extension of the leading edge; (2) formation and stabilization of new adhesive contacts; and (3) active contraction of the cortex and/or internal cytoplasm (Alberts et al., 1994; Bray, 2000; Lauffenberger and Horwitz, 1996; Mitchison and Cramer, 1996; Sheetz, 1994). Fig. 12D shows how the same processes might operate to drive convergent extension in the very different cellular, mechanical, and geometric context of a close-packed polarized monolayer epithelium. In this view, actin-dependent protrusive forces cause interior basolateral edges to extend across and between the interior faces of adjacent neighbors. To do so, the extending edge must displace existing adhesive connections between, and establish new adhesive contacts with, each of those neighbors. At the same time, cortical contractile forces operating away from the leading edge attempt to contract the cell boundary around an incompressible fluid volume.

Absent protrusive activity, contractile and hydrostatic forces will force cells towards isodiametric shapes. When protrusive forces deform a cell away from its preferred shape, contractile forces attempt to restore that shape. As local protrusive extension becomes biased to medial and lateral interior edges (Table 1), the contractile restoring force acting within each cell will also become biased perpendicular to the AP axis. Because contractile force will be roughly the same for neighboring cell boundaries, boundary shortening can occur without the need to make or break adhesive bonds. The only place where adhesive connections need break and reform is at or near three-cell junctions, where cells actively extend between neighbors.

The local result will be a steady movement of neighboring cells past one another through a combination of active local extension at three-cell junctions (which drives cells away from their preferred shapes), and coordinate contraction of neighboring cell boundaries elsewhere (which pulls cells back towards their preferred shapes). The global result will be chains of contractile cells, perpendicular to the AP axis, spanning the notochord plate's width, which contract to converge the notochord plate's width and thereby necessarily extend its length (Fig. 12E). As the ventral folds fuse, these contractile side-to-side chains become contractile rings encircling the

cylindrical rod, which squeeze it and cause it to extend anteriorly and posteriorly.

So long as mediolaterally biased protrusive extension persists, and unless resisted by some greater external force, mediolateral contraction and axial extension of the notochord will continue inevitably until every locally extending interior edge disappears (i.e. until every cell itself spans the entire width of the notochord plate or cross-sectional area of the notochord cylinder).

We have made and analyzed a mathematical model for cell rearrangements within epithelial sheets that incorporates detailed representations of the local protrusive, contractile and adhesive mechanics hypothesized above (Munro and Odell, unpublished). The results confirm our intuitive predictions outlined above and provide additional insights into the mechanics of cell rearrangement within epithelia. For example, they imply that the basal to apical flow of cortical and adhesive structures postulated by the cortical tractor model (Jacobson et al., 1986) would automatically result if protrusive activity were stronger basally than apically. Similarly, the biased coordinate contraction postulated by Fristrom (Fristrom, 1982) emerges as a secondary consequence of biased protrusive extension within the epithelial plane. Thus, rather than contradicting previous hypotheses, ours parsimoniously reconciles them within a single framework.

Active basolateral forces drive non-autonomous rearrangement of notochord cell apices

Our observations suggest that active forces generated below the apical surface drive a secondary 'passive' rearrangement of notochord cell apices. Apical domains elongate in the direction of tissue extension, a characteristic of non-autonomous forms of epithelial cell rearrangement (Honda et al., 1982; Keller and Hardin, 1987; Keller, 1978). Basolateral domains move relative to one another first and faster than apical domains even though the fractional rates (the absolute rate normalized by the cross-sectional cell length) are roughly equal, and the F-actin rich protrusions, which accompany and presumably drive basolateral extension, rarely if ever extend to the apical surface.

Apical rearrangement could be purely passive: i.e. active movement of basolateral domains towards (mediolaterally) or away from (along the AP axis) one another might simply pull the corresponding apices towards or away from one another. However if the apical cortex were contractile, then contractile forces could help drive rearrangements by forcing stretched apices back towards more isodiametric shapes as proposed above (Honda et al., 1984; Weliky and Oster, 1990).

Polarized basolateral extension may contribute to invagination

We have shown that active basolateral extension begins with, and continues through, the period of notochord plate invagination. If extension forces are stronger in the basolateral domain than apically as our data suggests, then they should contribute to invagination, for they will counteract the contractile forces which shorten cell boundaries more strongly basally than apically. If cortical contractile forces are everywhere equal, this would lead to a greater *net* constriction in apical cross sections which would help force an invagination.

Comparison to cellular mechanisms of convergent extension in *Xenopus laevis*

In *Xenopus laevis*, as in chick (Bancroft and Bellairs, 1976) and many of the teleost fishes (e.g. Cooper and Kimmel, 1998; Wood and Thorogood, 1994), the notochord forms from, and convergent extension occurs within, deep mesenchymal mesoderm that condenses secondarily during neurulation to form a cylindrical rod. Nevertheless, the cellular mechanisms underlying convergent extension of an epithelial sheet in ascidians are strikingly similar to those that occur in a mesenchymal context during gastrulation in *Xenopus laevis* [reviewed by Keller et al. (Keller et al., 1992)]. During gastrulation, somitic and chordamesodermal cells extend local mediolaterally directed protrusions across the surfaces of their neighbors, and the biased cellular traction forces that arise perpendicular to the AP axis give rise to contractile arcs of cells spanning the involuting marginal zone. These arcs form within pre-involuting tissue and subsequently move over the dorsal lip of the blastopore as part of the involution front. Shih and Keller suggest their contraction may drive involution as well as convergence and extension of dorsal mesoderm (Keller et al., 1992; Shih and Keller, 1992b). Later, when the *Xenopus* notochord becomes a cylindrical rod, these arcs become constriction rings as we have described here (Keller et al., 1989).

Together, the results we report here and those from Keller's lab point to a very general cellular mechanism of convergent extension, one conserved within the chordate phylum if not more broadly, and one that transcends differences between mesenchymal and epithelial germ layers. Our 'chains of contractile cells' above are Shih and Keller's 'arcs'. We suggest that this reflects an even deeper underlying conservation of the contractile, protrusive and adhesive machinery that cells use to move and change shape within embryos.

E. M. thanks Victoria Foe, Bill Moody and the members of his lab for sharing lab space, equipment and reagents during the course of this work. We thank George von Dassow and Victoria Foe for insights into fixing and visualizing the cytoskeleton, and George von Dassow for help with SEM. We thank Eli Meir, Billie Swalla, George von Dassow, Kristin Sherrard and several anonymous reviewers for insightful comments on the manuscript. E. M. was supported by an NSF predoctoral fellowship, and a predoctoral training grant in Molecular and Cell Biology from the NIH. E. M. dedicates this paper to Julie Coombs-Hahn, who first taught him to love sea squirts.

REFERENCES

- Alberts, B., Bray, D., Lewis, J., Raff, M., Roberts, K. and Watson, J. D. (1994). *Molecular Biology of the Cell*. New York: Garland.
- Bancroft, M. and Bellairs, R. (1976). The development of the notochord in the chick embryo, studied by scanning and transmission electron microscopy. *J. Embryol. Exp. Morphol.* **35**, 383-401.
- Bray, D. (2000). *Cell Movements*. 2nd Ed. New York and London: Garland Publishing.
- Bray, D. and White, J. G. (1988). Cortical flow in animal cells. *Science* **239**, 883-887.
- Brun, R. B. and Garson, J. A. (1984). Notochord formation in the mexican salamander (*Ambystoma mexicanum*) is different from notochord formation in *Xenopus laevis*. *J. Exp. Zool.* **229**, 235-240.
- Chen, W. T. (1981). Mechanism of retraction of the trailing edge during fibroblast movement. *J. Cell Biol.* **90**, 187-200.
- Cloney, R. A. (1964). Development of the ascidian notochord. *Acta Embryol. Morphol. Exp.* **7**, 111-130.

- Conklin, E. G.** (1905). The organization and cell lineage of the ascidian egg. *J. Acad. Nat. Sci.* **13**, 1-119.
- Conklin, E. G.** (1928). The embryology of amphioxus. *J. Morphol.* **54**, 69-151.
- Coombs, J. L., Villaz, M. and Moody, W. J.** (1992). Changes in voltage-dependent ion currents during meiosis and first mitosis in eggs of an ascidian. *Dev. Biol.* **153**, 272-282.
- Cooper, M. S. and Kimmel, C. B.** (1998). Morphogenetic cell behaviors and specification of cell fate during early teleost development. In *Motion Analysis of Living Cells* (ed. D. Soll), pp. 177-220. New York: Wiley-Liss.
- Elul, T., Koehl, M. A. and Keller, R.** (1997). Cellular mechanism underlying neural convergent extension in *Xenopus laevis* embryos. *Dev. Biol.* **191**, 243-258.
- Ettensohn, C. A.** (1985). Gastrulation in the sea urchin embryo is accompanied by the rearrangement of invaginating epithelial cells. *Dev. Biol.* **112**(2), 383-390.
- Foe, V. E., Field, C. M. and Odell, G. M.** (2000). Microtubules and mitotic cycle phase modulate spatiotemporal distributions of F-actin and myosin II in *Drosophila* syncytial blastoderm embryos. *Development* **127**, 1767-1787.
- Fristrom, D.** (1988). The cellular basis of epithelial morphogenesis. A review. *Tissue Cell* **20**, 645-690.
- Fristrom, D. K.** (1982). Septate junctions in imaginal discs of *Drosophila*: A model for the redistribution of septa during cell rearrangement. *J. Cell Biol.* **94**, 77-87.
- Fristrom, D. and Fristrom, J. W.** (1976). The mechanism of evagination of imaginal discs of *Drosophila melanogaster*. III. Evidence for cell rearrangements. *Dev. Biol.* **54**, 163-171.
- Gumbiner, B. M.** (1996). Cell adhesion: The molecular basis of tissue architecture and morphogenesis. *Cell* **84**, 345-357.
- Hardin, J.** (1989). Local shifts in position and polarized motility drive cell rearrangement during sea urchin gastrulation. *Dev. Biol.* **136**, 430-445.
- Honda, H., Ogita, Y., Higuchi, S. and Kani, K.** (1982). Cell movements in a living mammalian tissue: long-term observation of individual cells in wounded corneal endothelia of cats. *J. Morphol.* **174**(1), 25-39.
- Honda, H., Yamanaka, H. and Dan, S.-M.** (1984). A computer simulation of geometrical configurations during cell division. *J. Theor. Biol.* **106**, 423-435.
- Horowitz, P. and Hill, W.** (1989) *The Art of Electronics*, p. 991. Boston: Cambridge University Press.
- Jacobson, A. G., Oster, G. F., Odell, G. M. and Cheng, L. Y.** (1986). Neurulation and the cortical tractor model for epithelial folding. *J. Embryol. Exp. Morphol.* **96**, 19-49.
- Jay, P. Y., Pham, P. A., Wong, S. A. and Elson, E. L.** (1995). A mechanical function of myosin II in cell motility. *J. Cell. Sci.* **108**, 387-393.
- Keller, R. E.** (1978). Time-lapse cinematographic analysis of superficial cell behavior during and prior to gastrulation in *Xenopus laevis*. *J. Morphol.* **157**, 223-248.
- Keller, R. and Hardin, J.** (1987). Cell behaviour during active cell rearrangement: evidence and speculations. *J. Cell Sci. Suppl.* **8**, 369-393.
- Keller, R., Cooper, M. S., Danilchick, M., Tibbetts, P. and Wilson, P. A.** (1989). Cell Intercalation During Notochord Formation in *Xenopus laevis*. *J. Exp. Zool.* **251**, 134-154.
- Keller, R. E., Danilchick, M., Gimlich, R. and Shih, J.** (1985). The function and mechanism of convergent extension during gastrulation of *Xenopus laevis*. *J. Embryol. Exp. Morphol.* **89 Suppl**, 185-209.
- Keller, R., Shih, J. and Sater, A.** (1992). The cellular basis of the convergence and extension of the *Xenopus* neural plate. *Dev. Dyn.* **193**, 199-217.
- Kiehart, D. P.** (1982). Microinjection of echinoderm eggs: apparatus and procedures. *Method Cell. Biol.* **25**, 13-31.
- Kolega, J.** (1986). The cellular basis of epithelial morphogenesis. In *The Cellular Basis of Morphogenesis*, vol. 2 (ed. L. W. Browder), pp. 103-144. New York and London: Plenum Press.
- Lauffenberger, D. A. and Horwitz, A. F.** (1996). Cell migration: A physically integrated process. *Cell* **84**, 359-369.
- Lawson, M. A. and Maxfield, F. R.** (1995). Ca²⁺- and calcineurin-dependent recycling of an integrin to the front of migrating neutrophils. *Nature* **377**, 75-79.
- Lofberg, J.** (1974). Apical surface topography of invaginating and non-invaginating cells. a scanning-transmission study of amphibian neurulae. *Dev. Biol.* **36**, 311-329.
- Mitchison, T. J. and Cramer, L. P.** (1996). Actin-based cell motility and cell locomotion. *Cell* **84**, 371-379.
- Miyamoto, D. M. and Crowther, R. J.** (1985). Formation of the notochord in living ascidian embryos. *J. Embryol. Exp. Morphol.* **86**, 1-17.
- Nishida, H.** (1987). Cell lineage analysis in ascidian embryos by intracellular injection of a tracer enzyme. III. Up to the tissue restricted stage. *Dev. Biol.* **121**, 526-541.
- Owaribe, K., Kodama, R. and Eguchi, G.** (1981). Demonstration of contractility of circumferential actin bundles and its morphogenetic significance in pigmented epithelium in vitro and in vivo. *J. Cell Biol.* **90**, 507-514.
- Palecek, S. P., Schmidt, C. E., Lauffenberger, D. A. and Horwitz, A. F.** (1996). Integrin dynamics on the tail region of migrating fibroblasts. *J. Cell. Sci.* **109**, 941-952.
- Sardet, C., Speksnijder, J., Inoue, S. and Jaffe, L.** (1989). Fertilization and ooplasmic movements in the ascidian egg. *Ciba Found. Symp.* **105**, 237-249.
- Satoh, N.** (1993). *Developmental Biology of Ascidians*. Cambridge University Press.
- Schmidt, C. E., Dai, J., Lauffenberger, D. A., Sheetz, M. P. and Horwitz, A. F.** (1995). Integrin-cytoskeletal interactions in neuronal growth cones. *J. Neurosci.* **15**, 3400-3407.
- Schmidt, C. E., Horwitz, A. F., Lauffenberger, D. A. and Sheetz, M. P.** (1993). Integrin-cytoskeletal interactions in migrating fibroblasts are dynamic, asymmetric, and regulated. *J. Cell. Biol.* **123**, 977-991.
- Schoenwolf, G. C. and Alvarez, I. S.** (1989). Roles of neuroepithelial cell rearrangement and division in shaping of the avian neural plate. *Development* **106**, 427-439.
- Sheetz, M. P.** (1994). Cell migration by graded attachment to substrates and contraction. *Sem. Cell Biol.* **5**, 149-155.
- Shih, J. and Keller, R.** (1992a). Cell motility driving mediolateral intercalation in explants of *Xenopus laevis*. *Development* **116**, 901-914.
- Shih, J. and Keller, R.** (1992b). Patterns of cell motility in the organizer and dorsal mesoderm of *Xenopus laevis*. *Development* **116**, 915-930.
- Speigel, E. and Speigel, M.** (1986). Cell-cell interactions during sea urchin morphogenesis. In *The Cellular Basis of Morphogenesis*, vol. 2 (ed. L. W. Browder), pp. 195-240. New York and London: Plenum Press.
- Sulik, K., Dehart, D. B., Iangaki, T., Carson, J. L. and Vrablik, T.** (1994). Morphogenesis of the murinenode and the notochord plate. *Dev. Dyn.* **201**, 260-278.
- Thorogood, P. and Wood, A.** (1987). Analysis of In Vivo Cell Movement Using Transparent Tissue Systems. *J. Cell Sci. Suppl.* **8**, 395-413.
- Trinkaus, J. P., Trinkaus, M. and Fink, R. D.** (1992). On the convergent cell movements of gastrulation in *Fundulus*. *J. Exp. Zool.* **261**, 40-61.
- von Dassow, G. and Schubiger, G.** (1994). How an actin network might cause fountain streaming and nuclear migration in the syncytial *Drosophila* embryo. *J. Cell Biol.* **127**, 1637-1653.
- Warga, R. and Kimmel, C. B.** (1990). Cell movements during epiboly and gastrulation in the zebrafish. *Development* **108**, 569-580.
- Weliky, M. and Oster, G.** (1990). The mechanical basis of cell rearrangement. I. Epithelial morphogenesis during *Fundulus* epiboly. *Development* **109**, 373-386.
- Wood, A. and Thorogood, P.** (1994). Patterns of cell behavior underlying somitogenesis and notochord formation in intact vertebrate embryos. *Dev. Dyn.* **20**, 151-167.